Hindawi
International Transactions on Electrical Energy Systems
Volume 2022, Article ID 9995478, 17 pages
https://doi.org/10.1155/2022/9995478

Research Article

Identification of the Dominant Harmonic Source Type in the Distribution Network Using the Soft Computing Technique

Sasmita Lenka,[1] Pampa Sinha,[1] Kaushik Paul,[2] Chitrlekha Jena,[1] Swagat Das,[1] and Baseem Khan[3]

[1]*KIIT University, Bhubaneswar, India*
[2]*BIT Sindri, Dhanbad, India*
[3]*Department of Electrical and Computer Engineering, Hawassa University, Hawassa 05, Ethiopia*

Correspondence should be addressed to Baseem Khan; baseem.khan04@ieee.org

Received 10 June 2022; Revised 13 October 2022; Accepted 17 October 2022; Published 27 October 2022

Academic Editor: Michele De Santis

Copyright © 2022 Sasmita Lenka et al. This is an open access article distributed under the Creative Commons Attribution License, which permits unrestricted use, distribution, and reproduction in any medium, provided the original work is properly cited.

An innovative technique has been proposed for determining the position and characteristics of harmonic generating resources in a distribution system. The proposed methodology is primarily based on the wavelet decomposition of power signals on the factor of dimension. Detail power or harmonic power calculation at level 1 reduces the computational burden of the algorithm. The distinguishing harmonics concept can be used to detect a harmonic generating source from the distribution network. The sampling frequency is chosen so that the appropriate harmonic data are captured at level 1 and the pseudo-frequency of the wavelet decomposition at first level is close to the characteristic frequency of the load. The proposed method has been applied in different types of distribution systems to check its validity.

1. Introduction

In today's world, preserving the appropriate quality of voltage and current waveforms in the distribution system of the power system network has become a major challenge. The identification of participants closer to harmonic pollutants has become important; since the creation of deregulated power systems framework, the supplier of harmonics to an otherwise sinusoidal power system may be penalized and/or proper corrective measures may be initiated. In the recent times, issues related to the power quality, especially the identification of the sources for harmonic problems, have emerged as an integral topic for the power system researchers. Various methodologies for the detection of the harmonic source can be found in Refs. [1,2]. The approaches stated by most of the researchers in this field mainly deals with the development of the Thevenin or Norton equivalents that take into account the loads and sources, as well as the active nonactive power flows associated with the harmonics are also considered at the point of measurements. Authors of Ref. [3] discussed about the three major aspects pertaining to disturbance emission: (a) the location of disturbance sources, (b) the differentiation between the network and customer contribution to the emission level, and (c) the evaluation or assessment of the individual emission levels. This report focuses primarily on the final component. Experience with the application of emission level assessment guidelines in the context of postconnection investigations in order to determine whether the actual disturbance emission levels of a given installation conform to the IEC/TR limits or not. In Ref. [4] multichannel data acquisition systems and commercially available digital signal processing software packages are used to enable the determination of harmonic power flow. The authors explain how data from a typical acquisition system can be processed using the fast Fourier transform and also discuss potential errors (such as those caused by leakage) and how to avoid them using techniques such as skew correction and windowing. Presented are guidelines for the practical application of the transform in the analysis of measured data. The analysis method was successfully applied to data collected at a traction (railway

supply) substation with a sixth-harmonic resonance caused by the interaction of a harmonic filter and the sole supply system.

The ever-increasing number and power of polluting loads (nonlinear, time-varying loads) connected to the electric power network causes a significant distortion in the line current, as their combined power is no longer negligible in comparison to the network power, and also some distortion is seen in the line voltage. This degrades the quality of the electric power, which may disturb other connected loads. The availability of an instrument capable of quantifying the degradation of power quality due to harmonic distortion helps in determining whether or not this degradation is caused by a polluting load connected after the metering section and also in quantifying whether the effects of such a load is crucial for the proper operation of the electric power system. This paper [5] proposes a measurement method for identifying the source of pollution in a three-phase power system based on the evaluation of the harmonic powers. In order to quantify the electric power quality and the degrading effects of a polluting load, a number of parameters are also defined. A virtual instrument-realized digital instrument for implementing and experimentally validating the proposed method is also described. The precision of measurements is discussed in Ref. [5]. In a study [6], the authors have proposed a method for quantifying the distortion caused by a single customer in a network with multiple customers. They have described a technique for isolating the customer and supplier contributions to waveform distortion. The measurements of voltage and current at a single point are sufficient. This strategy is helpful in determining equitable methods for resolving customer complaints, such as sharing the cost of waveform distortion via rate structures or penalties.

In power quality, researchers suffered from the drawback that the sign of the harmonic power may be erroneous because of the near 90° phase shift between the harmonic voltage and currents. This problem has been addressed in Ref. [7], and a corrective solution related to the problem has been developed in which the determination of the harmonic power sign has been determined based on the time domain approach. The developed approach in their research has successfully identified the source of harmonics. Approaches that are based on the determination and measurements of nonactive power components do not involve the conducting of spectrum analysis of system voltage and current signal and therefore just require a basic measuring framework [8–11].

The authors of Refs. [12,13] proposed a methodology which is based on Thevenin/Norton equivalent of the input and output at each harmonic frequency, which makes this approach extremely time consuming to implement. A critical impedance approach was established in Ref. [14] to detect the principal source of harmonics by evaluating the magnitudes of harmonic voltage sources. This approach is also based in the computation of the Thevenin equivalents.

It is also difficult to divide the loads by categorizing them into the section of conforming and nonconforming components [15]. Additionally, these approaches categorize linear capacitive load with the nonlinear load which seems to be irrational. Summarizing, nonactive power-based methods may fail to identify whether the network or the loads are the contributors of harmonic at the threshold value of the indicator. These methods also fail to recognize the weak harmonic source [16].

Techniques that deal with the detection of total harmonic distortion (THD) is unable to ascertain the source of harmonic distortion effectively because they lack proper analysis of the phase angle deviation associated with the source of harmonics [17].

The power components involved in this field of research has been designated for sinusoidal current and voltage waveforms which have been found to be inadequate in depicting and portraying the system's operation under nonsinusoidal operating conditions. Thus, in Ref. [18], this inability has been eradicated with the illustration of new power components. The newly defined power component has been reformulated and specified with the utilization of the wavelet transform [19–22]. The present paper employs this wavelet-based power component to identify the location and type of the electrical component producing the harmonics. In Ref. [23], the authors have utilized the discrete wavelet transform to develop a method for the identification of the harmonic source. The proposed method in their research work portrays the computation of the detail power at the first level. The detail power basically extracts the harmonic power of frequency, dependent on the sampling frequency analysis in association with the analysis of the central frequency of the mother wavelet. The direction of flow of the detail power has been incorporated for the harmonic source location confirmation in reference to the measurement site. When there are many harmonic sources, the proposed method has been used to identify the dominating harmonic source. The paper[24] presented a novel transmission line approach.

The computer study of variational inequalities using a mean extra-gradient technique was given in Ref. [25]. The authors of Ref. [26] execute resource orchestration for cloud-edge-based smart grid fault detection. The data-driven dynamic harmonic model for contemporary home appliances was presented by the authors in Ref. [27]. The review of deep learning techniques used in frequency analysis and regulation of contemporary power systems was offered by the authors in Ref. [28]. The estimate of the probabilistic energy flow for the regional integrated energy system taking into account cross-system failures was given in Ref. [29]. The distributed model predictive control was suggested by the authors in Ref. [30] to use reactive power vehicles to the grid for real-time voltage adjustment in distribution networks. The characterization inference using joint optimization of multilayer semantics and deep fusion matching network was suggested by the authors in Ref. [31]. Based on a dynamic game strategy, writers in Ref. [32] devised voltage regulation using electric taxis. The domestic power load scenario forecast using a transferable flow generation model was given in Ref. [33]. In Ref. [34], authors presented the experimental set-up for the identification of power quality problems in the energy network interfaced with the

photovoltaic system. In Ref. [35], authors utilized the S-transform depended decision tree technique for the identification of complex power quality problems.

In Ref. [36], authors presented the novel technique to locate and find the type of the harmonics, generated in the distribution network. For that purpose, authors utilized the wavelet decomposition of current and voltage waveforms. For that purpose, loads which generated the harmonics are identified by extracting its characterizing harmonics. The characteristic frequency of the load serves as the pseudo-frequency for the wavelet decomposition at level 1, and the sampling frequency is selected in a way that allows for the extraction of the necessary harmonic information at level 1.

The basis of boundary protection is the detection of distinct frequency bands for the transient fault. The wavelet transform with db6 as the mother wavelet is utilized to capture two frequency bands from a transient current signal. The spectral energies of these two bands are extracted and utilized in order to determine whether the fault is located within or outside the protected zone. In Ref. [37], a hybrid time-frequency analysis method is presented that was developed specifically to decompose the time-varying harmonic subgroups and interharmonics of electric arc furnace (EAF) currents. The primary objective is accurate perception of harmonics and interharmonics in cases of rapid voltage or current changes or power quality (PQ) events. Using discrete wavelet transform (DWT), which provides time-localization for highly time-varying signals, it has been possible to detect harmonic and interharmonic frequencies. Although DWT produces accurate spectral decomposition at low frequencies, particularly at the baseband, as the bandwidths of the band-pass filters increase, the accuracy decreases at higher frequencies. To circumvent this issue, power signals are modulated with complex exponential waveforms, which corresponds to shifting the required harmonic subband contents to the baseband, where the DWT's accuracy is optimal.

The purpose of the proposed research work in this manuscript is to determine the nature of the harmonic source that occurs in radial and nonradial framework. The harmonic sources were identified by taking into account the source signal's harmonic nature. The signal was sampled at the optimum frequency depending on the frequency to be recorded, which was then used to acquire the detail power or harmonic power at the first level of wavelet decomposition. The theoretical framework and backdrop of the suggested technique are presented initially in this publication. The method for identifying harmonic sources is then discussed, and the methodology is supported by a one-of-a-kind case study.

Major contributions in this paper are (i) harmonic source identification based on their characteristics frequency, (ii) denoising of signal, (iii) selection of sampling frequency, (iv) introduced concept of frequency band to extract the signature of harmonic generating sources, (v) application of the proposed algorithm in different types of distribution systems to check its validity, and (vi) normalized entropy concept implementation. The direction of the fundamental active power flow is considered as the reference direction. The direction of the detail active power is considered to be positive if it is the same as that of the fundamental active power flow. That means in case of positive detail active power, the source of harmonic is in the upstream side (from where the active power comes) of the measurement point, and for negative detail active power, the harmonic source is in the downstream side (where the active power flows from the point of measurement) of the measuring point. The detail power at level 1, i.e., P_{det1} at a particular node decides whether the source of harmonic pollution is located upstream or downstream with respect to the point of measurement.

In order to facilitate the identification of the harmonic contributing source in a power network, a new method to identify the location and nature of the harmonic generating sources in a distribution system has been proposed in this paper. The method is based on the wavelet decomposition of the voltage and current signals at the point of measurement. Detail active power at level 1 of wavelet decomposition has been used. A harmonic generating load is identified by extracting its characterizing harmonics in the power system signals. The pseudo-frequency for the wavelet decomposition at level 1 is set at the characteristic frequency of the load, and the sampling frequency is so chosen that the desired harmonic information is extracted in detail at level 1. Power systems signals are however captured at a higher sampling frequency. For the identification of the disturbing source, the required sampling frequency for level one decomposition is obtained using the down sampling on the captured data. The applicability of the method has been demonstrated for both radial and nonradial power system networks.

2. The Proposed Methodology

2.1. Background. In Ref. [23], the authors have formulated a new approach for the harmonic source identification in the power system framework that deals with the wavelet transform. The approach has been inspired by the active power harmonic analysis based on the analysis of detail or harmonic active power in the wavelet domain [20].

Based on the discrete wavelet transform (DWT), the mathematical representation of the active power P can be represented as

$$P = \frac{1}{T}\int_0^T v(t)\cdot i(t)\mathrm{d}t, \tag{1}$$

where P can be segregated into components, which are approximate (P_{app}) and detail power (P_{detj}). Thus, P can be represented as

$$P = P_{\mathrm{app}} + P_{\mathrm{det}j}, \tag{2}$$

where

$$P_{\mathrm{app}} = \frac{1}{T}\sum C_{jo,k}C_{jo,k}^{'}, \tag{3}$$

$$P_{\mathrm{det}j} = \frac{1}{T}\sum_{j\geq j0}\sum_{k} d_{j,k}^{'}d_{j,k}. \tag{4}$$

The DWT coefficients related to the current and voltages are denoted as $C_{j0,k}$, $C'_{jo,k}$, respectively, corresponding to the scaling level $j0$ and the level of wavelet decomposition and is denoted as j. $d_{j,k}$, $d'_{j,k}$ represented in Ref. (4) resembles the DWT coefficient for current and voltage, respectively, at k^{th} sample. In Refs. (5) and (6), the RMS values of the voltage and current signals corresponding to specific frequency band are marked as V_j and I_j which resembled the detailed voltage (V_{det}) and detailed current (I_{det}), respectively:

$$V_{\det j} = \frac{1}{\sqrt{T}} \sqrt{\sum_{j \geq j0} \sum_{k} d'} \tag{5}$$

$$I_{\det j} = \frac{1}{\sqrt{T}} \sqrt{\sum_{j \geq j0} \sum_{k} d}, \tag{6}$$

$$\begin{aligned} C'_{j0,k} &= v(t), \quad \varphi j_{j0,k}, \\ d'_{j0,k} &= v(t), \quad \varphi j_{j0,k}, \end{aligned} \tag{7}$$

$$\begin{aligned} C_{j0,k} &= i(t), \quad \varphi j_{j0,k}, \\ d_{j0,k} &= i(t), \quad \varphi j_{j0,k}. \end{aligned} \tag{8}$$

In Equations (7) and (8), and the scaling function is represented as $\varphi_{j0,k}$, and $\psi_{j,k}$ represents the wavelet basis function [20].

The formula for detail active power at level 1 is given in eq. (9) as P_{det1}:

$$P_{\det j} = \frac{1}{T} \sum_{j \geq j0} \sum_{k} d'_{1,k} d_{1,k}. \tag{9}$$

In Equation (9), the DWT coefficient for current is represented as $d_{1,k}$ and for voltage is represented as $d'_{1,k}$ corresponding to the 1^{st} decomposition level and k^{th} sample.

P_{det1} resembles the detail active power at level 1, which is associated to a specified node that determines whether the location of the source of harmonic pollution is located at the downstream or upstream considering the node as the reference. At a specific point within the considered system, if the value of P_{det1} is positive, then it signifies that the harmonic power has been received from the upstream side with respect to the point of measurement. Similarly, when the value of P_{det1} resembles a negative sign, then it is considered that the harmonic power is obtained from the downstream side. In the case when there is more than one harmonic source present, then a conflicting situation arises. In such a scenario, the identification of the stronger harmonic source is done by determining the pollution power (DP) level of the source. The source which is highlighting higher value of DP is treated as the dominant supplier of harmonics. The dominant source of harmonic pollution location can be determined taking into consideration the signs of the detail power for the scenario when single nonlinear load or more than one nonlinear loads are present.

2.2. Specific Harmonic Source Identification Based on the Selection of Signature Harmonic Frequency. In general, the source's characteristic harmonic information is utilized as the fundamental concept of governing the detection of the kind of harmonic generating source. Such data are easily accessible for typically used distribution system loads. The power electronic loads are considered to be the primary producers of harmonics in power systems framework and mostly produce odd harmonics. This scenario can be practically observed in the case of a 6-pulse converter that bears a significant amount of 5^{th} and 7^{th} harmonic components, and both 11^{th} and 13^{th} components of the harmonics are dominant for 6-pulse converters as well as for 12-pulse converters. It is also seen that triplen harmonics are present in case of the transformer exciting current. Hence, it can be observed that based on the characterizing harmonics, the identification of a particular disturbing load can performed.

Table 1 presents the comparative analysis at the 1^{st} level of decomposition between pseudo and sampling frequency. The proposed method, the wavelet analysis of the active power signal at detail level 1, has been utilized to search the frequency. The information related to the desired harmonic power is achieved based upon the adjustment performed in the sampling frequency. In this paper, the optimum sampling frequency can be described as the sampling frequency that facilitates the extraction of the information related to the corresponding harmonic information at detail level 1. Obviously, the optimum sampling frequency will depend upon the frequency of the signal to be extracted and also on the central frequency of the mother wavelet chosen.

2.3. Optimum Sampling Frequency for Finding Out the Different Types of Harmonic Generating Sources. The frequency information from the coefficient extracted at the j^{th} decomposition level in case of the wavelet decomposition can be represented as

$$F_{psj} = \frac{F_c \cdot F_s}{2^j}, \tag{10}$$

where the pseudo-frequency at the j^{th} level is given as F_{psj}, F_s resembles the sampling frequency, and the frequency of mother wavelet, that is, central frequency related to the selected wavelet is represented as F_c [11]. The mother wavelet db10 has been used in this study as this has been found to be the most suitable mother wavelet for steady state power system distorted waveform analysis [38]. F_{psj} resembles the frequency band around the frequency F_{psj} even if it has a single frequency value. The computation of the sampling frequency can be done considering the information related to the pseudofrequency that have been fetched regarding the signature harmonics of the voltage/current signal. The proposed approach portrays the search of the characterizing frequency bands based on the decomposition of the power signal for the distribution system loads. The voltage and current have 50 Hz as the fundamental frequency, and the active power signal exhibits a 100 Hz frequency. Accordingly, for the third harmonic, the frequency of the active power component is 300 Hz.

Table 1: Comparative analysis at the 1st level of decomposition between pseudo-frequency and sampling frequency.

Specific harmonic	Captured power frequency (Hz)	Sampling frequency (Hz)
3rd	300	877
5th	500	1461.56
7th	700	2046.185
9th	900	2630.8
11th	1100	3215.43
13th	1300	3800

Thus, the determination of sampling frequency in case of the fundamental active power extraction at the level 1 of the discrete wavelet transform can be represented as

$$Fs = \frac{2 \times Fps_j}{0.6842}. \tag{11}$$

The pseudo-frequency, and the sampling frequency corresponding to each harmonic level has been shown in Table 1 for Daubechies 10 (db10) mother wavelet and the decomposition at the first level.

The frequency band estimation included in a wavelet analysis with specific frequency F_{psj} of level j is represented as

$$Fps_j = \frac{(m+1)F_s}{2^{j+1}}, \quad j = 1, \ldots J-1, \tag{12}$$

where F_s is denoted as the sampling frequency and J is the last decomposition level. The range of m is denoted as $m = 0, 1, \ldots 2^{j-1}$ and $m = 0$, 1 for DWT [39]. A simulation in MATLAB 2021 has been conducted for a network energized with a nonsinusoidal voltage source which has all odd harmonics up to the 19th order in order to further verify the above condition. The network's loads are considered to be linear, in the present work. Table 2 shows the proportion of harmonic power computed by P_{det1} at sampling frequencies of 877 Hz, 1461 Hz, and 3800 Hz. These frequencies resemble the specific pseudo-frequencies of 3rd, 5th, and 13th harmonic powers, respectively. At a sampling frequency of 1461 Hz, which corresponds to the 5th harmonic power, P_{det1} can determine the 5th harmonic power. P_{det1} calculates 85.26% of the 3rd harmonic power, 83.24% of the 7th harmonic power, and 20.46% of the 9th harmonic power at this sampling frequency, with the influence of other harmonic powers minimal. Similarly, at 877 Hz sampling frequency, P_{det1} only records 100% of the 3rd harmonic power and 20% of the 5th harmonic power. Table 2 also shows the contributions of the harmonic powers on P_{det1} at 3800 Hz sampling frequency. The above analysis serves as the foundation for the harmonic source detection strategy in our suggested method. The main concept deals with the pseudo-frequency selection that aids in the detection of the source. Subsequently, the sampling frequency must be selected so that the extraction of the pseudo-frequency component can be done at level 1 of wavelet. The characteristic pseudo-frequency must be chosen with care in order to encompass the bulk of the harmonics created by the harmonic generator and gather their contributions to the extracted coefficient for the purpose of detecting the harmonic source. As a result, the sample frequencies must be modified based on the defining harmonics of the targeted harmonic generating sources, as various harmonic sources may have different characteristics frequencies. Table 2 presents different values of p_{det1} at various sampling frequencies.

Table 2: Different values of pdet1 at various sampling frequencies.

Harmonic order	$F_s = 1461$ Hz	$F_s = 877$ Hz	$F_s = 3800$ Hz
Fundamental	1.05	3.9	0.12
3rd order harmonic	86.5	100	0.76
5th order harmonic	100	19.5	1.96
7th order harmonic	86.7	—	5.89
9th order harmonic	19.78	—	19.89
11th order harmonic	—	—	83.6
13th order harmonic	—	—	100
15th order harmonic	—	—	82.6
17th order harmonic	—	—	42.5
19th order harmonic	—	—	12.5

3. Validation of the Proposed Technique

This section of the manuscript highlights the determination of various forms of harmonic generating sources existing in the power system radial network based on the different sampling frequencies as shown in Figure 1.

The framework of the radial network bears five nodes which are demarcated as *A, B, C, D,* and *Y*. Each of the node is also accompanied with a load. In the considered framework, the fundamental frequency internal impedance of the voltage source Z_S has been taken as $(1 + j6.28)\ \Omega$ with $(1 + j12.56)\ \Omega$ as the value corresponding to the line impedance. In this work, loads Z_1, Z_2, Z_3,and Z_4 are assigned the fundamental frequency impedance of $(100 + j\ 62.8)\ \Omega$.

The proposed approach is validated for two types of loads. The first scenario takes into account the nonlinear load characterized by single frequency, and in the second scenario, the multiple frequencies can characterized the load.

(i) Case I: Since it is known that the load will produce a certain harmonic component, the wavelet pseudo-frequency adjustments become necessary, and it must be adjusted equivalent to the harmonic frequency that will best characterize the nonlinear load. Table 2 demonstrates that in such case studies, the wavelet decomposition is able to capture 100% of the harmonic content of the power system signal in addition to other side frequency signals that are present in the signals. Therefore, the wavelet decomposition will specifically extract the harmonic content of the load signal whenever single harmonic component is produced by the nonlinear load.

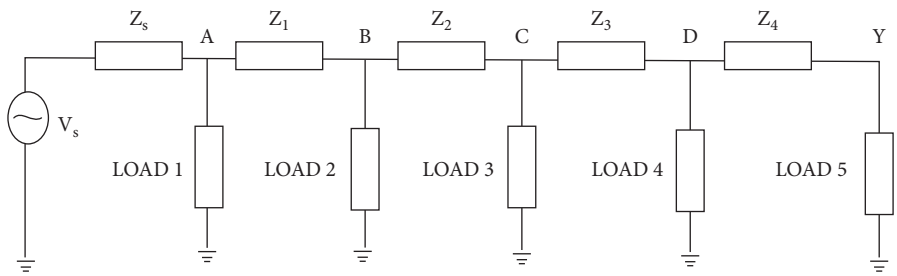

Figure 1: Representation of the linear and nonlinear loads in a framework of radial network.

3.1. Determination of Load Delivering 3rd Harmonic Current. To validate the proposed technique, a nonlinear load that contributes a third harmonic component has been first attached at node C of the considered distribution system, with the other linear loads. The modeling of the connected nonlinear load has been done by the current source, and in this case, the value of the 3rd harmonic current has been achieved to be equal to 60% of the fundamental current that is given by the load. A frequency of 877 Hz has been determined to be the sample frequency that corresponds to the pseudo-frequency of the 3rd harmonic power. Table 3 demonstrates in detail the active power measured at level 1 (denoted by P_{det1}) across all of the nodes, with the assumption that the sampling frequency is 877 Hz. The results of the FFT demonstrate that the power computed with the incorporation of the wavelet transform and the harmonic power estimated from FFT are quite similar to one another and agree very closely. In this case, FFT has been computed exclusively for the 3rd harmonic power, and it has been realized that P_{det1} computes the third harmonic power at 877 Hz of sampling frequency. It has been seen that the value of P_{det1} is negative which signifies that the 3rd harmonic power which has been delivered by the disrupting load is located downstream (based on Node *C*), and it is positioned at upstream when node *D* and *Y* are taken as reference node. This is indicated by the fact that P_{det1} is negative up to node *C*. As a result, node *C* highlights the dominant harmonic location [40].

3.2. Detection of Load Promoting 5th Harmonic Current. We are now considering the connected nonlinear load at the position C to be a source of the 5th harmonic current rather than the 3rd harmonic current. The analysis of the power signal has been performed considering sampling frequency to be 1461 Hz which corresponds to the pseudo-frequency of the 5th harmonic power. From Table 4, it can be noted that at a sample frequency of 1461 Hz, P_{det1} is negative up to node C. As a result, the position of the harmonic source has been accurately established. Moreover, the magnitude of the 5th harmonic current has also been calculated correctly as observed from the FFT values.

(i) Case II: Ideally, the characterization of the load is done by more than one harmonic order, and the pseudo-frequency needs to be set so that it is in the middle of the characterizing harmonic frequencies. This allows the DWT to capture an adequate quantity of the harmonic information of the power signal that is derived by the load. In most cases, the harmonic frequencies are adjacent odd order frequencies. In the case of a six-pulse converter, for instance, the fifth and seventh harmonics are the primary components of the current waveform. Even if the even harmonics are not present in the signal at this time, the pseudo-frequency need to be fixed at the frequency of the sixth harmonics, and the optimal sampling frequency ought to be established in accordance with this. The wavelet decomposition, in this instance, catches 96 percent of the fifth harmonic and 97 percent of the 7th harmonic, respectively. In a similar manner, in order to identify the 12-pulse converter, the pseudo-frequencies set at the 12th order harmonic must be used, with the 11th and 13th harmonics serving as the primary distinguishing frequencies for the 12-pulse converter. Two examples of loads delivering multiple frequencies are shown below.

3.3. Determination of Loads Delivering 3rd and 5th Harmonic Current. Figure 2 displays three graphical representation of curves that illustrate the harmonic contents that have been recorded by the wavelet decomposition at level 1 when the adjustments of the pseudo-frequencies are achieved in relation to 3rd, 4th, and 5th harmonics, respectively. It is possible to detect the sample frequency that corresponds to the 4th order of harmonics to track the significant components of the harmonic frequencies that belong to the 3rd and 5th order of harmonic. Therefore, the pseudo-frequency that corresponds to the fourth harmonic should be able to capture the harmonic features of the load; the third and fifth harmonics being the typical harmonic frequencies of the load. The outcomes of P_{det1} are shown in Table 5 for the network depicted in Figure 1. The outcomes are achieved when 3rd and 5th harmonic promoting nonlinear loads are coupled at the location of node C. The 3rd harmonic current comprises 60% of the fundamental frequency current, and the 5th harmonic component comprises 20% of the fundamental frequency current. When the active power signal is evaluated taking into consideration the sampling frequency of 877 Hz, the location and amplitude of the source of the 3rd harmonic are found. When the signal is evaluated using a sample frequency of 1461 Hz, the location and amplitude of the source of the 5th harmonic may be determined. Now the signal is decomposed at a sample frequency of 1169 Hz,

Table 3: 3rd harmonic current component contributed by the nonlinear load.

Nodes	FFT Values	DWT(P_{det1}) Values $F_s = 877$ Hz	% Error	Conclusion
A	−2.7	−2.65		
B	−7.55	−7.38		
C	−18.45	−18.51	1.25	Node C is the harmonic source
D	8.58	8.74		
Y	3.21	3.27		

Table 4: 5th harmonic current component contributed by the nonlinear load.

Name of the node	FFT values	DWT(P_{det1}) Values $F_s = 1461$ Hz	% Error	Conclusion
A	−2.79	−2.66		
B	−7.56	−7.605		
C	−18.42	−18.62	1.974	Node C is the location for the harmonic source
D	8.56	8.68		
Y	3.2	3.25		

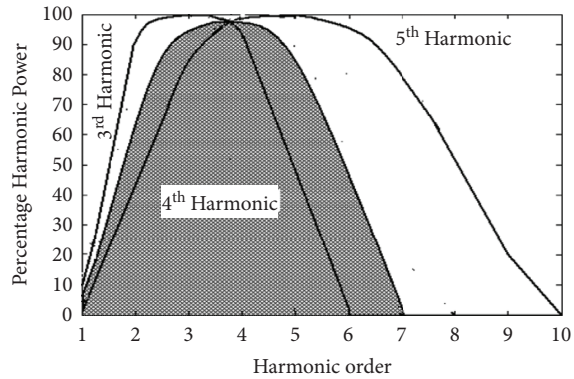

Figure 2: Pseudo-frequency vs. captured harmonic power for 3rd, 4th, and 5th harmonics.

which is located in the middle of the two sampling frequencies mentioned previously and relates to 4th harmonic power.

From Table 5, it can be observed that at this sampling frequency, P_{det1} has the third and the fifth component of harmonic power. Therefore, the location of a harmonic source that delivers both a third and fifth harmonic component may be detected by using P_{det1} at a sampling frequency that corresponds to fourth harmonic power. It is important to take note of the fact that the presence of third and fifth order harmonics may be determined from a single decomposition by utilizing a sample frequency of 1169 Hz (pseudo-frequency for the 4th harmonics).

3.4. Determination of Loads Delivering 11th and 13th Harmonic Current. The decomposed wavelet component records the frequency content that is depicted in Figure 3 when the adjustments in the pseudo-frequencies are done in relation to the 11th, 12th, and 13th harmonics, respectively. The image makes it abundantly clear that the pseudo-frequency of the 12th order harmonics is capable of capturing significant proportion of the 11th and 13th order harmonics. Because of this, the pseudo-frequency is adjusted to 12th harmonic in order to recognize loads whose primary characteristic harmonics are of the 11th and 13th order. Let us assume that the nonlinear load positioned at the location of node C depicted in Figure 1 is now delivering harmonic current of the 11th and 13th order. The associated findings are presented in Table 6 below. The current at the 11th harmonic is equal to 10% of the current at the fundamental frequency, and the current at the 13th harmonic is equal to five percent of that current. This current is given by the load that is linked to node C. In the process of analyzing the active power signal at sampling frequencies of 3215 Hz and 3800 Hz, the position and amplitude of the 11th and 13th harmonics power are determined, respectively.

When P_{det1} is calculated with a sampling frequency of 3507 Hz which relates to the 12th harmonic power, in this scenario, both the 11th and 13th harmonic powers are calculated by P_{det1}, as observed from Table 6. Again, it is evident from Table 6 that presence of 11th and 13th order harmonics may be identified from a single decomposition at sampling frequency 3507 Hz, i.e., corresponding to the 12th order harmonic.

3.5. Determination of a Thyristor-Controlled Load. Table 7 presents the results of determining the harmonic power impact of a thyristor-controlled single-phase bridge rectifier load that is located at node C. The FFT has been utilized to individually compute the 3rd, 5th, 7th, 9th, and 11th harmonic powers and are represented in Table 7. It is abundantly obvious that the principal frequency components of the thyristor-controlled load consist mostly of the third and fifth harmonics. Consequently, it is possible to recognize this load by utilizing wavelet decomposition to obtain the pseudo-frequency components that correspond to the fourth harmonic. The P_{det1} values for a variety of sample frequencies are presented in Table 7 below. It is clear that P_{det1} values are the largest for sampling frequency 1169 Hz, which corresponds to the 4th harmonic power. Hence, the identification of the load is performed based on the active power at level 1 with sampling frequency 1169 Hz.

Table 5: The 3rd and 5th harmonic current generated by the load.

Node name	Determined FFT values		Determined DWT (P_{det1}) values		
	3rd harmonic	5th harmonic	*Fs* = 877 Hz	*Fs* = 1461 Hz	*Fs* = 1169 Hz
A	−2.7	−0.83	−2.65	−0.89	−3.21
B	−7.55	−0.79	−7.38	−0.7587	−8.11
C	−18.45	−2.13	−18.51	−2.13	−20.56
D	8.58	0.99	8.74	1.03	9.78
Y	3.21	0.38	3.27	0.38	3.48

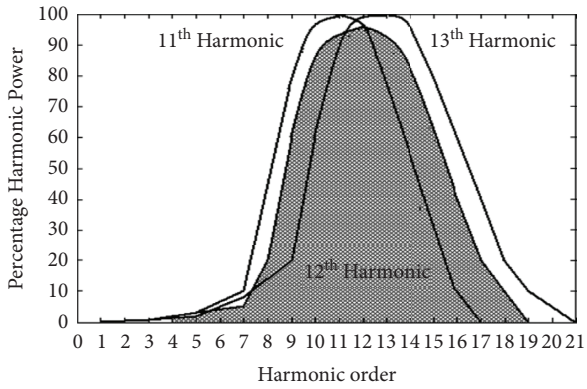

Figure 3: Representation of the 11th, 12th, and 13th harmonics pseudo-frequency vs. captured harmonic power.

4. Signal Denoising

Influence of Noise In Real-Time System. The voltage and current signals are always contaminated with noise. Noise, or interference, can be defined as undesirable electrical signals, which distort or interfere with an original (or desired) signal. Hence, the effectiveness of the proposed method for detection of HIF has been studied under noisy environment also. The noise in power system is present throughout the whole recorded signal and has normal probability distribution. This noise is specified by the signal-to noise ratio (SNR) expression where

$$\mathrm{SNR}_{dB} = 20\log_{10}\left(\frac{A_{\mathrm{signal}}}{A_{\mathrm{noise}}}\right). \tag{13}$$

As the proposed work uses the DWT-based technique, denoising is a very important issue. After denoising, the signal harmonics can be extracted which will give more accurate results. In Figure 4, the short circuit fault current signal has been shown. Figures 5 and 6 are noisy signal and denoise signal, respectively.

5. Implementation of the Proposed Method

The proposed approach in this research work can be implemented to determine the position of the nonlinear load based on the flowchart, as represented in Figure 7. To illustrate the proposed concept, test results are presented for the radial and nonradial power system network.

5.1. Application to the Radial Network. Two different case studies are considered. The network shown in Figure 1 is considered for analysis. Two cases are analyzed so as to investigate the capability of the proposed method for the position identification of the 6-pulse and 12-pulse converters. For the 6-pulse converters, the major frequency contents are the 5th and 7th harmonics though there are traces of other harmonic like 11th and 13th . Thus, selecting the pseudo-frequency at the midway between the 5th and 7th harmonic, i.e., at the 6th harmonic frequencies, the 6-pulse converter may be identified.

Figure 8 shows three curves representing the harmonic contains obtained by the wavelet decomposition at detail level 1 when pseudo-frequencies values are adjusted in relation to 5th, 6th, and 7th harmonic frequencies.

The corresponding sampling frequency is 1753 Hz. The 12-pulse converter on the other hand has major frequency contents at the 11th and 13th order harmonics. Thus, the identification of 12-pulse converter is achieved by setting the pseudo-frequency value to the 12th harmonic and accordingly selecting the sampling frequency at 3507 Hz. It may be noted that the 6-pulse converter also contains the 11th and 13th harmonics, but these harmonics are not used to identify the converter as the 5th and 7th harmonics are the major constituents.

(i) Case I: In the first case study, a 6-pulse converter and a 12-pulse converter have been taken which are connected at node D and node B, respectively, along with one 3rd harmonic source at C. Table 8 shows P_{det1} at different nodes for this case study. It can be seen that the value of P_{det1} is negative up to node C corresponding to the sampling frequency of 877 Hz, indicating the presence of the 3rd harmonic source at the downstream side of node C. Again, P_{det1} is negative up to node D at the sampling frequency 1753 Hz, indicating the presence of 6-pulse converter downstream with respect to node D. The sign of P_{det1} at 3507 Hz indicates the presence of converter on both sides of node C. As 12-pulse converters do not generate 5th or 7th harmonic power, its presence is not indicated at 1753 Hz and is only indicated at 3507 Hz. Hence, node B is associated with the 12-pulse converter. The direction for the flow of P_{det1} for different harmonic levels is shown in Figure 9.

Table 6: The 11th and 13th harmonic current generated by the load.

Name of the node	FFT values		DWT (P_{det1}) values		
	11^{th} harmonic	13^{th} harmonic	$Fs = 3215$ Hz	$Fs = 3800$ Hz	$Fs = 3507$ Hz
A	−1.32	−0.41	−1.3	−0.39	−1.65
B	−2.34	−0.6	−2.31	−0.57	−2.81
C	−4.51	−1.21	−4.46	−1.19	−5.72
D	2.05	0.45	2.1	0.41	2.5
Y	1.18	0.12	1.19	0.13	1.3

(ii) Case II**:** Table 9 highlights the results related to the second case study. In this case, the 6-pulse converter has been taken into consideration along with the 12-pulse converter which are connected at the position of node B and node D, respectively, along with the 3^{rd} harmonic current source at node C. P_{det1} corresponding to the sampling frequency of 1753 Hz shows that the 6-pulse converter generating the 5^{th} and 7^{th} harmonic power is located at the position of node B. P_{det1} corresponding to sampling frequency of 3507 Hz reveals that the harmonic source generating the 11^{th} and 13^{th} harmonic is located on both sides of node C. As the node D does not generate the 5^{th} or 7^{th} harmonic power, so it can be concluded that the position of the 12-pulse converter is at node D. The presence of third harmonic source at node C is observed due to the negative sign of P_{det1} up to node C indicating the presence of third harmonic current source at node C. The directions of flow of P_{det1} for different harmonic levels are shown in Figure 10.

(iii) Case III: Table 10 highlights the results related to the third case study. In this case, two 6-pulse converters have been taken into consideration which are connected at the position of node B and node D with different firing angle, i.e., 20° and 60°, respectively. P_{det1} corresponding to the sampling frequency of 1753 Hz shows that the 6-pulse converter generating the 5^{th} and 7^{th} harmonic power is located at the position of node B and D. Due to higher firing angle, node D is more dominating; hence, the direction of harmonic active power flow is in the upstream side. Based on Table 10, F_s corresponding to the 6^{th} harmonic shows being negative up to node D and F_s corresponding to the 12^{th} order harmonics is also negative up to node D. Hence, through this method, only a dominating harmonic generating source can be identified. According to this table, the direction of harmonic active power is opposite to the fundamental active power. Hence, as 6-pulse converters connected at node D is most dominating, so harmonic active power flows from node D to the grid side. So, the bus magnitude of P_{det1} is very high and then goes on decreasing, but as another 6-pulse converter is connected at node B, hence the magnitude of P_{det1} gets boosted up. From this, we can conclude that this network contains two number of 6-pulse converters.

5.2. Proposed Approach Implementation and Analysis for Nonradial Network. In this section, the framework of nonradial power system network has been considered to evaluate the applicability of the proposed approach. In order to analyze the proposed approach, a 4-bus nonradial network has been opted and has been represented in Figure 11. Bus 1 has a sinusoidal supply of 230 Volts, 50 Hertz that has an internal impedance of $(1+j6.28)\ \Omega$, and each of the transmission line of the 4-bus system has an impedance of $(1 + j12.56)\ \Omega$. In addition to this, a linear load of $-100+j62.8\ \Omega$ is connected at bus 2 along with a linear load of $-(150 + j78.5)\ \Omega$ at bus 3 and bus 4 has a $(75 + j47)\ \Omega$ impedance. Apart from this configuration, bus 3 has a 3^{rd} harmonic source attached to it, bus 2 and bus 4 have 6-pulse and 12-pulse converters attached to it, respectively. The detail power flow based on the varying sampling frequency at level 1 has been represented in Table 11. The corresponding detail powers at different buses are shown in Table 12. The 3^{rd} harmonic power flow can be determined from P_{det1} corresponding to sampling frequency 877 Hz. The 5^{th} and 7^{th} harmonic power flows are observed from P_{det1} corresponding to sampling frequency of 1753 Hz, and the 11^{th} and 13^{th} harmonic power is determined at sampling frequency of 3507 Hz. In an interconnected system, if the detail power at level 1, i.e., P_{det1} and approximate power P_{app} in a particular transmission line is flowing in the same direction, then the source of harmonic pollution is considered to be located in the upstream side. If the detail power flows opposite to the direction of approximation power, then the source of harmonic pollution is located in the downstream side. At a particular bus, the incoming power is considered to be negative. Hence, when detail power connected to a particular bus is negative, it indicates that the bus is receiving harmonic power and is polluted by the network. The outgoing power connected to a bus is considered to be positive. Hence, positive detail power at a bus indicates that the bus is delivering harmonic power and polluting the system network. It is shown in Table 11 that the bus 3 delivering 3^{rd} harmonic power as P_{det1} is positive at bus 3 at sampling frequency 877 Hz, and all other buses absorb this power. The positive sign of P_{det1} at bus 2 corresponding to 1753 Hz sampling frequency indicates that bus 2 delivers the 5^{th} and 7^{th} harmonic power. Again corresponding to the sampling frequency of 3507 Hz, it is observed that both bus 2 and bus 4 deliver the 11^{th} and 13^{th} harmonic powers. Thus, based on the category of the harmonic powers associated at the buses, it can be understood that bus 2 has a 6-pulse converter and bus 4 has a 12-pulse converter.

Table 7: FFT and DWT results of the thyristor-controlled load.

Node position	FFT values achieved for the proposed approach					DWT values achieved for the proposed approach					
	3^{rd} harmonic	5^{th} harmonic	7^{th} harmonic	9^{th} harmonic	11^{th} harmonic	$F_s = 877$ Hz	$F_s = 1169$ Hz	$F_s = 1461$ Hz	$F_s = 2046$ Hz	$F_s = 2630$ Hz	$F_s = 3215$ Hz
A	−0.18	−0.069	−0.105	-2.9×10^{-2}	−0.0156	−0.16	−0.192	−0.0498	−0.16	−0.016	−0.0157
B	−2.204	−0.425	−0.158	−0.148	−0.064	−2.12	−2.15	−0.06069	−0.14	−0.1447	−0.0438
C	−6.13	−1.206	−0.528	−0.42	−0.197	−6.13	−7.5	−1.65	−0.686	−0.39	−0.1128
D	2.508	0.819	0.16	0.074	0.102	2.418	3.2	0.809	0.162	0.068	0.109
Y	0.939	0.2098	0.06	0.022	0.03	0.899	1.18	0.3093	0.041	0.021	0.0218

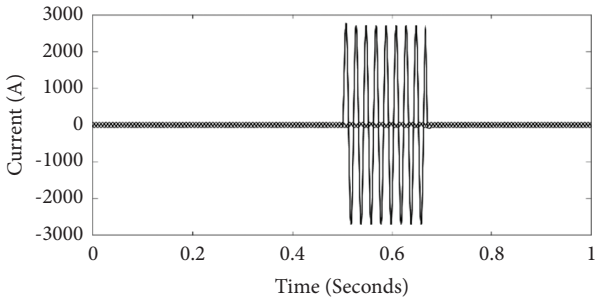

Figure 4: current signal during short circuit fault.

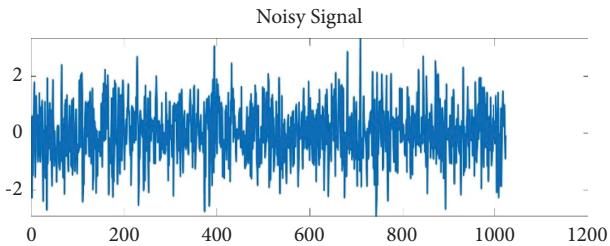

Figure 5: External noise signal.

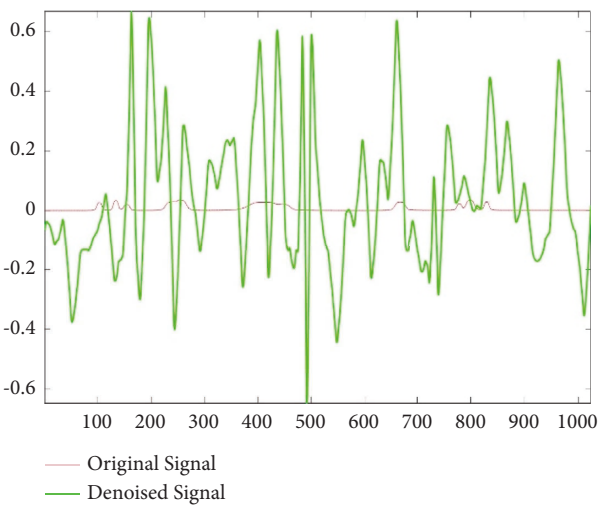

Figure 6: current signal during short circuit fault after denoising and applied DWT.

6. Integration of Distributed Generation in Radial Distribution System

To connect this distributed generation (DG) to the power system, it is necessary to understand the voltage and power profile of the distribution system at each bus. In this paper, a backward-forward sweep analysis of load flow is utilized. Load flow analysis is performed in MATLAB. The appendix contains the line data and load data of the IEEE33 radial distribution bus. The power flow problem has reached convergence, with a convergence value of less than 0.001. Bus 18 is observed to have a low voltage of 0.9136 p.u, and bus 33 is also observed to have a low voltage of 0.917 p.u. These buses are considered to be weak buses, and distributed generators can be introduced to meet the load demand. The fundamental objective function for optimal DG sizes is as follows:

$$\text{Minimize} P_L = \sum_{i=1}^{n} |i_i|^2 R_i, \tag{14}$$

subjected to

$$|V_{i\min}| \le |V_i| \le |V_{i\max}|. \tag{15}$$

$$|I_{ij}| \le |I_{ij\max}|, \tag{16}$$

where P_L represents power loss, and power loss must be minimized. R_i is the resistance of the ith branch. I_i is the current flowing through the ith branch. In this case, bus 18 and bus 33 are deemed the optimal locations for distribution generation placement. Using a PSO-based optimization technique, the DG sizing problem is optimized. Using the IEEE33 bus radial distribution test system, this optimization problem is resolved. The DG size and power loss obtained following optimization are shown in Table 13.

In this paper, a PV module with integrated battery is used as a distributed generation source. The power loss is reduced from 203 kilowatts to 90.3 kilowatts. The total amount of energy saved by this DG placement is 113 kW. The PV rating at bus 33 is 1.2 MW, and the PV rating at bus 18 is 0.65 kW. These distributed generation (DG) sources are introduced at bus 18 and bus 33. On the block diagram, the weak buses 16, 17, 18 and 31, 32, 33 are indicated with a red colour. Figure 12 depicts the block diagram of IEEE33 radial distribution system with DG.

The PV module integrated with the battery source is designed and simulated in MATLAB simulink. The MATLAB simulink model of a PV cell integrated with the battery source is shown in Figure 12.

7. Entropy Calculation

An entropy provides information about uncertainty of the signal and the quantity of signal. As a result, entropy measurement provides information on signal defects. The measurement of entropy begins with the computation of wavelet energy. The energy entropy can reflect arc voltage properties, and the energy entropy (E_i) formula is expressed by

$$\text{Sum of Energies} E_i = |C_i(t)|^2, \tag{17}$$

where $C_i(t)$ are the high frequency detail coefficients of the DWT transform extracted arc voltage, and i are the number of extraction levels. In this method, the no. of level is 1, and coefficients are collected corresponding to 4^{th} and 12^{th} order harmonics. The energy distribution is now expressed as the ratio of the energies corresponding to the 4^{th} and 12^{th} order harmonics, and the energy of the subband signal is defined as

$$P_i = \frac{E_i}{E},$$
$$E = \sum_{i=1}^{n} E_i. \tag{18}$$

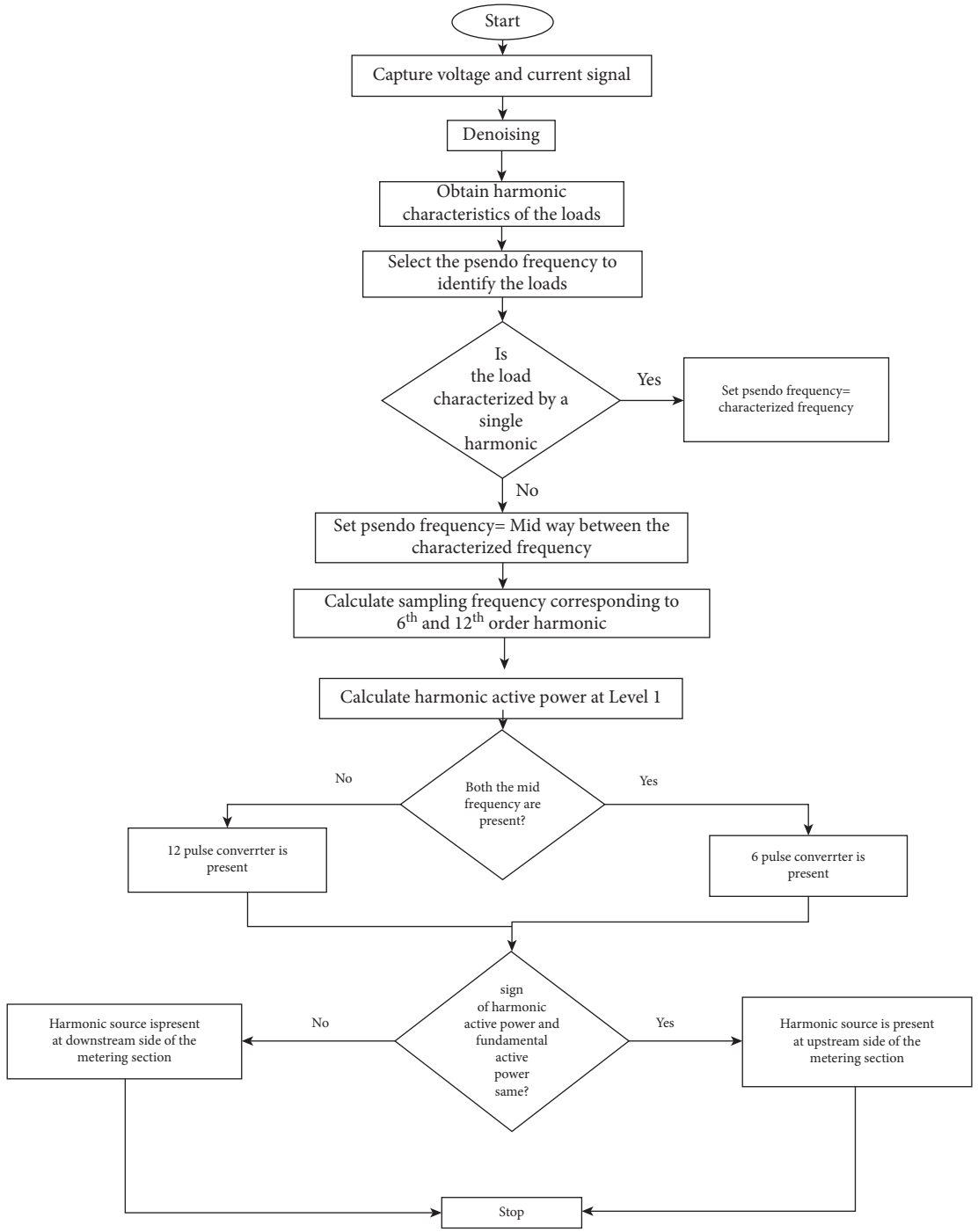

Figure 7: Flowchart of the source identification algorithm.

The spectral entropy of a signal based on wavelet theory is mathematically denoted as

$$E_{\text{Spectral}} = -\sum_{m=1}^{N} P_i \log_2 (P_i). \tag{19}$$

In order to scale the entropy data and organize in a structured way, entropy values are scaled from the range 0 to 1. This process is known as normalization. Normalization is done by dividing spectral entropy with the logarithm of N, where N is the number of frequency points or half of the length of the time series. This has been represented as

$$\text{Normalized} E_{\text{Spectral}} = \frac{E_{\text{Spectral}}}{\log_2 (N)}. \tag{20}$$

Since the proposed normalized values provide sufficient discrimination between different types disturbances, based on Table 14, different types of harmonics generating sources can be identified.

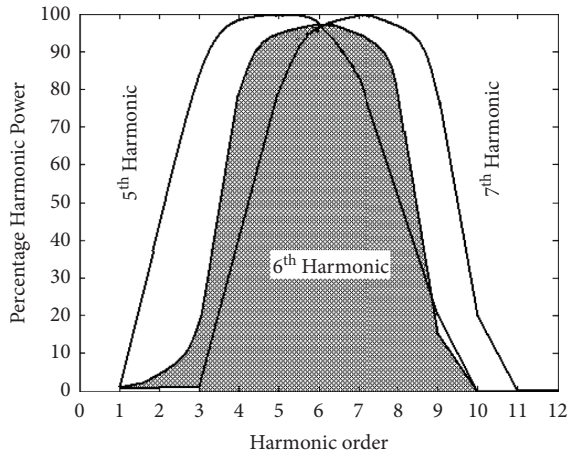

Figure 8: Pseudo-frequency vs. captured harmonic power for 5th, 6th,7th harmonics.

Table 8: DWT outcomes for 6-pulse and 12-pulse converter positioned at node D node B, respectively.

Node	$Fs = 877$ Hz	$Fs = 1753$ Hz	$Fs = 3507$ Hz
A	−0.26	−2.32	−0.51
B	−0.56	−7.65	−1.46
C	−1.12	2.24	0.4
D	0.63	0.601	−0.106
Y	0.42	0.12	0.318

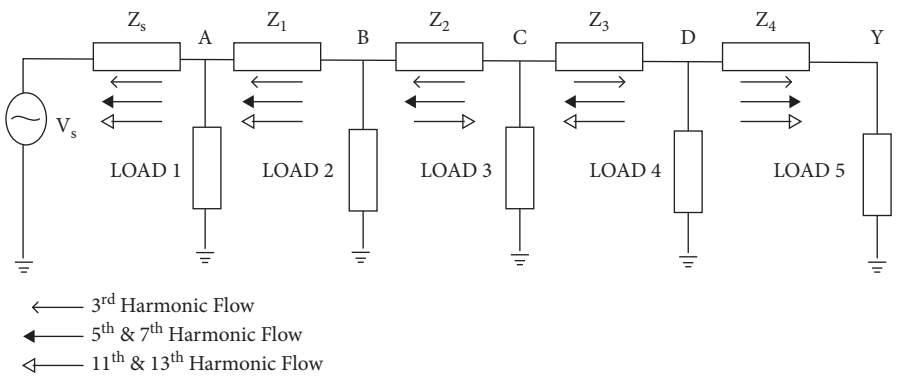

Figure 9: Harmonic power flow representation with 6-pulse and 12-pulse converter (at Node *D* and Node *B*, respectively) along with one 3rd harmonic source at *C*.

Table 9: Outcomes of 6-pulse and 12-pulse converter connected at node *B* and node *D*, respectively, with DWT.

Node	$Fs = 877$ Hz	$Fs = 1753$ Hz	$Fs = 3507$ Hz
A	−0.95	−0.15	−0.71
B	−1.53	−0.35	−0.92
C	−1.86	−0.61	0.36
D	0.92	−2.16	−0.86
Y	0.75	0.92	0.09

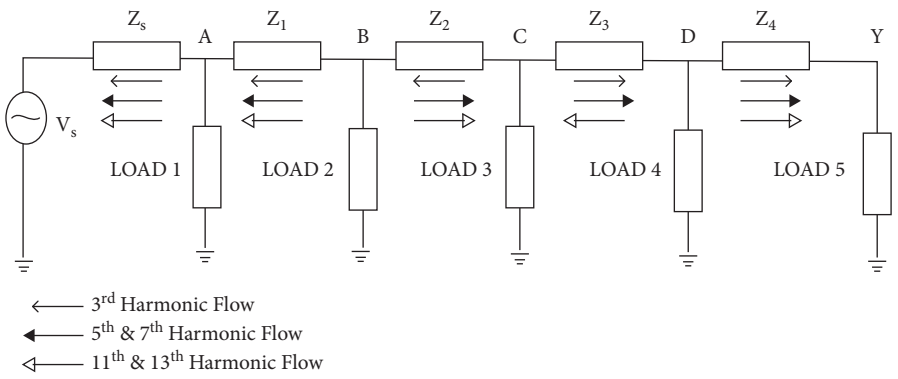

Figure 10: Harmonic power flow representation with 6-pulse and 12-pulse converters (at Node *B* and Node *D* respectively) along with one 3rd harmonic source at *C*.

Table 10: Outcomes of two 6-pulse converters connected at node *B* and node *D*, respectively.

Node	*Fs* = 1753 Hz	*Fs* = 3507 Hz
A	−0.18	−0.43
B	−0.56	−0.56
C	−0.69	0.54
D	−2.89	−0.91
Y	0.92	0.09

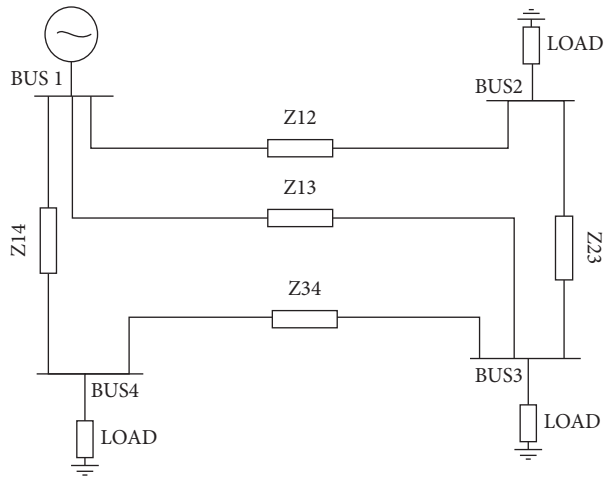

Figure 11: Nonradial network.

Table 11: Nonradial network line power flow with DWT.

Line	*Fs* = 877 Hz	*Fs* = 1753 Hz	*Fs* = 3507 Hz
1–2	−7.02	−26.21	−3.17
2–1	8.55	35.29	4.34
2–3	−9.8	42.93	8.18
3–2	10.48	−40.21	−7.88
3–4	12.13	21.21	−2.28
4–3	−9.01	−16.25	2.73
4–1	3.96	11.29	8.74
1–4	−3.29	−9.21	−5.97
1–3	−11.21	2.19	−4.18
3–1	17.19	−1.12	5.51

Table 12: Nonradial network bus power flow with DWT.

Bus	$Fs = 877$ Hz	$Fs = 1753$ Hz	$Fs = 3507$ Hz
1	−21.52	−33.23	−13.32
2	−1.25	78.22	12.52
3	39.8	−20.12	−4.65
4	−5.05	−4.96	11.47

Table 13: DG sizing.

Bus number	Voltage profile before DG	Voltage profile after DG	Power loss	DG size
33	0.917	0.967	90.3 kw	1.2 MW
18	0.9136	0.963	90.3 kw	0.65 MW

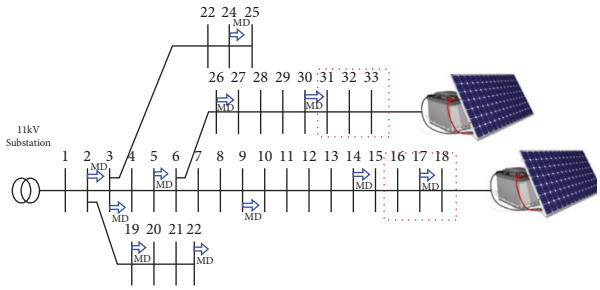

Figure 12: Block diagram of IEEE33 Bus with Distributed Generation.

Table 14: Mean entropy values of various fault conditions.

Grid type	Mean entropy									
	4^{th} order	12^{th} order	4^{th} order	12^{th} order	4^{th} order	12^{th} order	4^{th} order	12^{th} order	4^{th} order	12^{th} order
Type of distribution grid	SC fault		Capacitor Switching Transients		Load Switching Transients		Feeder Energization transients		DG generated harmonics	
	0.815	0.72	0.81	0.99	0.681	0.561	0.886	0.68	0.54	0.71
Modified IEEE33 BUS	0.815	0.72	0.81	0.99	0.681	0.561	0.886	0.68	0.54	0.71

8. Conclusion

In this research manuscript, a novel approach has been proposed for identifying the region and kind of nonlinear loads observed in the deregulated framework of the power system. It is an enhancement of the approach previously proposed with the aid of the authors for the detection of harmonic resources which is based totally on the route of the flow of the detail power. At the first level of decomposition, the active power signal is decomposed using wavelet decomposition with specified sampling frequencies of the harmonic polluting source with a specific mother wavelet to recover the frequency composition information associated with the performance of the disturbing load. This approach has been utilized to identify kind disturbing load and its location in the power system distribution network. The evaluation of the efficacy of the proposed method has been examined on the different power system model including DG in the IEEE33 bus system. To identify the different harmonic generating sources in the power system, the normalized entropy concept has been utilized by different types of disturbances can be identified irrespective of voltage levels.The results achieved with the implementation of the proposed approach highlights that it bears the potential to effectively identify the category of the disturbing load in the distribution framework of the power system.

Data Availability

Data will be available on request. For the data related query, kindly contact Baseem Khan (baseem.khan04@ieee.org).

Conflicts of Interest

The authors declare that they have no conflicts of interest.

References

[1] P. H. Swart, M. J. Case, and J. D. van Wyk, "On techniques for localization of sources producing distortion in electric power networks," *European Transactions on Electrical Power*, vol. 4, pp. 485–489.

[2] T. Tanaka and H. Akagi, "A new method of harmonic power detection based on the instantaneous active power in three phase circuits," *IEEE Transactions on Power Delivery*, vol. 10, no. 4, pp. 1737–1742, 1995.

[3] CIGRE 36.05/CIRED 2 Joint Working Group CC02 (Voltage Quality), *Review of Methods for Measurement and Evalution of Harmonic Emission Level from an Individual Distortion Load*, CIGRE, Paris, France, 1999.

[4] T. A. George and D. Bones, "Harmonic power flow determination using the fast Fourier transform," *IEEE Transactions on Power Delivery*, vol. 6, no. 2, pp. 530–535, 1991.

[5] L. Cristaldi and A. Ferrero, "A method and related digital instrument for the measurement of the electric power quality," *IEEE Transactions on Power Delivery*, vol. 10, no. 3, pp. 1183–1189, 1995.

[6] K. Srinivasan, "On separating customer and supply side harmonic contributions," *IEEE Transactions on Power Delivery*, vol. 11, no. 2, pp. 1003–1012, 1996.

[7] W. A. Omran, S. Hamdy, K. El-Goharey, M. Kazerani, and M. M. A. Salama, "Identification and measurement of harmonic pollution for radial and nonradial systems," *IEEE Transactions on Power Delivery*, vol. 24, no. 3, pp. 1642–1650, 2009.

[8] P. V. Barbaro, A. Cataliotti, V. Cosentino, and S. Nuccio, "A novel approach based on nonactive power for the identification of distributing loads in power systems," *IEEE Transactions on Power Delivery*, vol. 22, no. 3, pp. 1782–1789, 2007.

[9] A. Cataliotti, V. Cosentino, and S. Nuccio, "Comparison of nonactive power for the detection of dominant harmonic sources in power systems," *IEEE Transactions on Instrumentation and Measurement*, vol. 57, no. 8, pp. 1554–1561, 2008.

[10] A. Cataliotti and V. Cosentino, "Distributing load identification in power systems: a single-point time-domain method based on IEEE 1459-2000," *IEEE Transactions on Instrumentation and Measurement*, vol. 58, no. 5, pp. 1436–1445, May 2009.

[11] A. Cataliotti and V. Cosentino, "A new measurement method for detection of harmonic source in power system based on the approach of IEEE Std. 1459-2000," *IEEE Transactions on Power Delivery*, vol. 25, no. 1, pp. 332–340, 2010.

[12] W. Xu and Y. Liu, "A method for determining customer and utility harmonic contributions at the point of common coupling," *IEEE Transactions on Power Delivery*, vol. 15, no. 2, pp. 804–811, 2000.

[13] N. Hamzah, Mohamed, and A. Hussain, "Harmonic source location at the point of common coupling based on voltage magnitude," in *Proceedings of the 2004 IEEE Region 10 Conference TENCON 2004*, Chiang Mai, Thailand, 2004.

[14] C. Chen, X. Liu, Koval, W. Xu, and T. Tayjasanant, "Critical impedance method- a new detecting harmonic sources method in distribution systems," *IEEE Transactions on Power Delivery*, vol. 19, no. 1, pp. 288–297, Jan. 2004.

[15] K. Srinivasan, "Conforminf and non conforming current for attributing steady state power quality problems," *IEEE Transactions on Power Delivery*, vol. 13, no. 1, pp. 212–217, 1998.

[16] M. Farhoodnea, A. Mohamed, shareef Hussain, and H. Zayandehroodi, "An enhanced method for contribution assessment of utility and customer harmonic distortions in radial and weakly meshed distribution systems," *International Journal of Electrical Power and Energy Systems*, vol. 43, no. 1, pp. 222–229, Dec. 2012.

[17] Sergio Ferreirade Poula Silva and Jose Carlos de Oliveira, "The sharing of responsibility between the supplier and the consumer for harmonic voltage distortion: a case study," *Electric Power Systems Research*, vol. 78, no. 11, pp. 1959–1964, 2008.

[18] "Definitions for the measurements of electric quantities under sinusoidal, non-sinusoidal, balanced, or unbalanced conditions," *IEEE Std*, vol. 1459-2000, 2010.

[19] W. G. Morsi and M. E. Ei- Hawary, "Defining power components in nonsinusoidal unbalanced polyphase systems: the Issues," *IEEE Transactions on Power Delivery*, vol. 22, no. 4, pp. 2428–22438, 2007.

[20] W. G. Morsi and M. E. Ei- Hawary, "Reformulating power components definitions contained in the IEEE Standard 1459-2000 using discrete wavelet transform," *IEEE Transactions on Power Delivery*, vol. 22, no. 3, pp. 1910–1916, 2007.

[21] W. G. Morsi and M. E. Ei- Hawary, "Reformulating three-phase power components definitions contained in the IEEE standard 1459-2000 using discrete wavelet transform," *IEEE Transactions on Power Delivery*, vol. 22, no. 3, pp. 1917–1925, 2007.

[22] F. Vatansever and A. Ozdermir, "Power parameters calculations based on wavelet packet transform," *International Journal of Electrical Power and Energy Systems*, vol. 31, no. 10, pp. 596–603, 2009.

[23] S. Nath, P. Sinha, and S. K. Goswami, "A wavelet based novel method for the detection of harmonic sources in power systems," *International Journal of Electrical Power & Energy Systems*, vol. 40, no. 1, pp. 54–61, 2012.

[24] B. Hu, Y. Tang, Q. Niu, Z. Shi, Y. Han, and X. Li, "Exploring spatial-temporal multi-frequency analysis for high-fidelity and temporal-consistency video prediction," in *Proccedings of the IEEE/CVF Conference on Computer Vision and Pattern Recognition (CVPR)*, Seattle, WA, USA, 2020.

[25] T. Cai, D. Yu, H. Liu, and F. Gao, "Computational analysis of variational inequalities using mean extra-gradient approach," *Mathematics*, vol. 10, no. 13, p. 2318, 2022.

[26] J. Li, Y. Deng, W. Sun et al., "Resource orchestration of cloud-edge–based smart grid fault detection," *ACM Transactions on Sensor Networks*, vol. 18, no. 3, 2022.

[27] X. Xie and D. Chen, "Data-driven dynamic harmonic model for modern household appliances," *Applied Energy*, vol. 312, 2022.

[28] Y. Zhang, X. Shi, H. Zhang, Y. Cao, and V. Terzija, "Review on deep learning applications in frequency analysis and control of modern power system," *International Journal of Electrical Power & Energy Systems*, vol. 136, Article ID 107744, 2022.

[29] H. Li, K. Hou, X. Xu, H. Jia, L. Zhu, and Y. Mu, "Probabilistic energy flow calculation for regional integrated energy system considering cross-system failures," *Applied Energy*, vol. 308, Article ID 118326, 2022.

[30] J. Hu, C. Ye, Y. Ding, J. Tang, and S. Liu, "A distributed MPC to exploit reactive power V2G for real-time voltage regulation in distribution networks," *IEEE Transactions on Smart Grid*, vol. 1, 2021.

[31] W. Zheng and L. Yin, "Characterization inference based on joint-optimization of multi-layer semantics and deep fusion matching network," *PeerJ Computer Science*, vol. 8, no. e908, 2022.

[32] K. Hu, X. Yue, Y. Wang, J. Yang, H. Zhao, and Z. Liu, "Voltage regulation with electric taxi based on dynamic game strategy," *IEEE Transactions on Vehicular Technology*, vol. 71, no. 3, pp. 2413–2426, March 2022.

[33] L. Lin, C. Chen, and B. Wei, "Residential electricity load scenario prediction based on transferable flow generation model," *J. Electr. Eng. Technol*, 2022.

[34] A. G. Shaik, N. Gupta, M. Khosravy, B. Khan, H. H. Alhelou, and S. Padmanaban, "Recognition of power quality issues associated with grid integrated solar photovoltaic plant in experimental framework," *IEEE Systems Journal*, vol. 15, no. 3, pp. 3740–3748, 2021.

[35] O. P. Mahela, A. G. Shaik, B. Khan, R. Mahla, and H. H. Alhelou, "Recognition of complex power quality disturbances using S-transform based ruled decision tree," *IEEE Access*, vol. 8, pp. 173530–173547, 2020.

[36] P. Sinha, S. K. Goswami, and S. Nath, "Wavelet-based technique for identification of harmonic source in distribution system," *International Transactions on Electrical Energy Systems*, vol. 26, pp. 2552–2572, 2016.

[37] E. Sezgin and Ö. Salor, "Analysis of power system harmonic subgroups of the electric arc furnace currents based on a hybrid time-frequency analysis method," *IEEE Transactions on Industry Applications*, vol. 55, no. 4, pp. 4398–4406, 2019.

[38] W. G. Morsi and M. E. Ei- Hawar, "The most suitable mother wavelet for steady state power system distorted waveforms," in *Proceedings of the IEEE Canadian Conference on Electrical and Computer Engineering (CCECE 08)*, Niagara Falls, Ontario Canada, May 2008.

[39] S. Bilgin, O. H. Colak, E. Koklukaya, and N. Ari, "Efficient solution for frequency band decomposition problem using wavelet packet in HRV," *Digital Signal Processing*, vol. 18, no. 6, pp. 892–899, 2008.

[40] H. Ahmed Sher, K. E. Addoweesh, and Y. Khan, "Harmonics Generation, Propagation and Purging Techniques in Non-Linear Loads," *An Update on Power Quality*, 2013, London, United Kingdom, IntechOpen, https://www.intechopen.com/chapters/43901.